3D Seismic Inversion by Model Parameterization with Fourier Coefficients

Fengxia Gao, Ying Rao, Tong Zhu, and Yanghua Wang

Abstract—In seismic inversion, the subsurface model can be parameterized by a truncated Fourier series, and the inversion problem is then the inversion of the Fourier coefficients. To improve the efficiency of the evaluation of the Fourier coefficients and the reconstruction of the model from the inverted coefficients, we propose to use the efficient implementation of the fast Fourier transform (FFT) to speed up these two calculations. By using the FFT pair, the computation time for 3D subsurface models with realistic size could be reduced by two to three orders of magnitude compared to conventional methods. When this model parameterization scheme is applied to seismic impedance inversion, we proposed two strategies to further improve the efficiency. One is to invert the Fourier coefficients from small-valued numbers to large-valued numbers, and the other is to divide the seismic data into subgroups and use part of them for the inversion of the Fourier coefficients. Both strategies are helpful for efficient inversion of the Fourier coefficients from the seismic data. Moreover, thanks to this model parameterization scheme, the Fourier coefficients are inverted in a multi-trace manner, and the impedance model reconstructed from the inverted Fourier coefficients has good spatial continuity. The scheme is able to generate stable and continuous impedance models from the inversion of seismic data with missing traces, with affordable computation times.

Index Terms—Fourier series, Fourier transform, seismic inversion, model parameterization.

I. INTRODUCTION

I N seismic inversion, different wavelength components of the earth subsurface model have different sensitivities [1]. Therefore, Wang and Houseman [2], [3] proposed to parameterize the subsurface model by a truncated Fourier series, partition the Fourier coefficients into different subspaces according to their wavelengths, and develop a subspace inversion algorithm for simultaneous inversion of the long, medium and short wavelength components of the subsurface model. This model parameterization scheme, which uses a truncated Fourier series, has been successfully

F. Gao is with SinoProbe Center, Chinese Academy of Geological Sciences and China Geological Survey, Beijing 100037, China. (e-mail: fengxia_gao@hotmail.com).

Y. Rao is with College of Geophysics, China University of Petroleum (Beijing), Beijing 102249, China. (e-mail: raoying@cup.edu.cn).

T. Zhu is with Sinopec Geophysical Research Institute Co. Ltd., Nanjing 21103, China. (e-mail: zhutong.swty@sinopec.com).

Y. Wang is with Centre for Reservoir Geophysics, Resource Geophysics Academy, Imperial College London, London SW7 2BP, UK. (e-mail: yanghua.wang@imperial.ac.uk).

applied to the joint inversion of seismic traveltime and amplitude data for interface geometry and velocity variation [3], [4], [5], waveform inversion for a two-dimensional (2D) impedance model [6], and inversion of amplitude variation versus offset (AVO) for elastic parameters [7].

In this model parameterization scheme, after parameterizing the subsurface model with a truncated Fourier series, the problem of inverting the subsurface model is transformed into the problem of inverting the Fourier coefficients. This model parameterization has obvious advantages. One of them, as with other model parameterizations based on the wavelet transform [8] or the cosine function [9], [10], is that fewer parameters need to be inverted compared to the total number of parameters of the subsurface model. By increasing the number of Fourier coefficients, a hierarchical strategy for stepwise inversion of the subsurface model is developed. Other advantages are the spatial continuity of the inverted subsurface model due to the reconstruction of the model from the Fourier coefficients and the implementation of a multi-trace inversion scheme due to the updating of the Fourier coefficients using all or part of the seismic data [6]. This multi-trace inversion scheme is insensitive to noisy data, and is therefore useful to obtain robust and stable models. Apart from the above advantages of model parameterization, we can use only seismic data within the region of interest in the truncated Fourier series coefficient inversion to save computational time. Nunes et al. [11] used a one-dimensional (1D) Fourier series to reduce the data size and simulated each term of the Fourier series over the region of interest, achieving a significant cost reduction in seismic inversion. In addition, this parameterization scheme lends itself to parallel computation during inversion, resulting in further savings in computation time. Due to these advantages, this model parameterization scheme has great potential for seismic inversion and is useful for subsurface model inversion.

However, when this model parameterization is applied to 3D seismic inversion, it is limited by the large amount of time required to evaluate the Fourier coefficients and reconstruct the subsurface model from the Fourier coefficients. This is because the two processes are conventionally realized directly by equations defining the Fourier coefficients (see appendix), and the subsurface model (see second section), which requires many integrations [12]. Although the time required for 1D/2D seismic inversion is acceptable, it is not sustainable for realistic 3D seismic inversion. This is because the 3D subsurface model has model samples along the three directions, and the integrations for coefficient estimation and model reconstruction are performed in three loops along these

directions, which increases the computational time cost. In addition, the subsurface model must be reconstructed from the Fourier coefficients for the wavefield simulation in each iteration. Its computation time is proportional to the time cost for the inversion. Therefore, it is necessary to speed up these two processes to improve the computational efficiency and make the Fourier series-based parameterization scheme practical for 3D seismic inversion. In this paper, we present the Fourier transform-based methods for computing the Fourier coefficients and reconstructing the model. Here, we use the fast implementation of the forward and inverse Fourier transforms to perform the model fitting and reconstruction.

With a fast implementation of Fourier coefficient estimation and model reconstruction, this model parameterization scheme is flexible in seismic inversion, and suitable for both prestack and post-stack seismic data [6], [7]. Here it is used for the inversion of the 3D impedance model from the post-stack seismic cube, which contains some randomly distributed null traces. This means that no data were recorded in these traces, because the sources/receivers are poor or the areas are unsuitable for setting sources/receivers during seismic acquisition. Impedance inversion was chosen for the application because impedance is an important parameter for reservoir description and detection, and because post-stack inversion is computationally efficient compared to pre-stack data, which is convenient for testing inversion strategies and inverted models using the parameterization scheme.

To sum up, we will first present a model parameterization scheme based on the truncated Fourier series for a 3D subsurface model. Secondly, we will propose to use the fast Fourier transform (FFT) to compute the coefficients of the truncated Fourier series and to use the inverse FFT to reconstruct a 3D model from the inverted coefficients of a truncated Fourier series. Thirdly, we will compare the computation time for the coefficient evaluation and for the 3D model reconstruction between the proposed FFT-based methods and the conventional direct computation methods. Finally, we will demonstrate the applicability of the method for seismic impedance inversion using examples for a 3D overthrust model and a field dataset. In the application section, we will develop inversion strategies based on the model parameterization scheme to further improve the computational efficiency.

II. MODEL PARAMETERIZATION BY THE FOURIER SERIES

The 3D subsurface model is parameterized by a truncated Fourier series. Considering a discrete 3D model with limited samples (N_x, N_y, N_z) in (x, y, z) directions, the truncated Fourier series can be expressed as follows:

$$\hat{u}(p,q,r) = \sum_{(l,m,n)=(0,0,0)}^{(L-1,M-1,N-1)} \varphi_{lmn}(p,q,r), \tag{1}$$

where $\hat{u}(p,q,r) \equiv \hat{u}(p\Delta x, q\Delta y, r\Delta z)$,

$$
\begin{aligned}
\varphi_{lmn}(p,q,r) &= a_{lmn}\cos(l\Delta k_x p)\cos(m\Delta k_y q)\cos(n\Delta k_z r) \\
&+ b_{lmn}\sin(l\Delta k_x p)\cos(m\Delta k_y q)\cos(n\Delta k_z r) \\
&+ c_{lmn}\cos(l\Delta k_x p)\sin(m\Delta k_y q)\cos(n\Delta k_z r) \\
&+ d_{lmn}\sin(l\Delta k_x p)\sin(m\Delta k_y q)\cos(n\Delta k_z r) \\
&+ e_{lmn}\cos(l\Delta k_x p)\cos(m\Delta k_y q)\sin(n\Delta k_z r) \\
&+ f_{lmn}\sin(l\Delta k_x p)\cos(m\Delta k_y q)\sin(n\Delta k_z r) \\
&+ g_{lmn}\cos(l\Delta k_x p)\sin(m\Delta k_y q)\sin(n\Delta k_z r) \\
&+ h_{lmn}\sin(l\Delta k_x p)\sin(m\Delta k_y q)\sin(n\Delta k_z r).
\end{aligned}
\tag{2}
$$

In this expression, $\{a,b,\cdots,h\}$ with subscripts $\{l,m,n\}$ are the $\{l,m,n\}$ th Fourier coefficients, (L,M,N) are the number of Fourier coefficients in the three dimensions, resulting in total number of Fourier coefficients in (1) is $8 \times L \times M \times N$, and $(\Delta k_x, \Delta k_y, \Delta k_z)$ are the fundamental wavenumbers, set as

$$\Delta k_x = \frac{2\pi}{N_x}, \quad \Delta k_y = \frac{2\pi}{N_y}, \quad \Delta k_z = \frac{2\pi}{N_z}. \tag{3}$$

The Fourier series representation $\hat{u}(p,q,r)$ is an approximation to the true model $u(p,q,r) \equiv u(p\Delta x, q\Delta y, r\Delta z)$ because the Fourier series expansion is truncated. The Fourier coefficients $\{a_{lmn}, b_{lmn}, \cdots, h_{lmn}\}$ can be calculated by integrating the product of $u(p,q,r)$ with certain sine and cosine functions. See the Appendix for the derivation process of the equations for the Fourier coefficients. In these equations, the coefficients of the truncated Fourier series that are not zero are the following:

$$
\begin{bmatrix}
\{a_{000},\, a_{l00},\, a_{0m0},\, a_{00n},\, a_{l0n},\, a_{lm0}, a_{0mn}, a_{lmn}\} \\
\{b_{l00},\, b_{lm0},\, b_{l0n}, b_{lmn}\} \\
\{c_{0m0},\, c_{lm0},\, c_{0mn}, c_{lmn}\} \\
\{d_{lm0},\, d_{lmn}\} \\
\{e_{00n},\, e_{l0n},\, e_{0mn}, e_{lmn}\} \\
\{f_{l0n},\, f_{lmn}\} \\
\{g_{0mn},\, g_{lmn}\} \\
\{h_{lmn}\}
\end{bmatrix}. \tag{4}
$$

It is obvious that the direct evaluation of the Fourier coefficients (with (A-1) to (A-6) in appendix) and the reconstruction of the model from (1) are very time-consuming, which may limit the application of model parameterization with truncated Fourier series in seismic inversions. To speed up the evaluation of the Fourier coefficients and the model reconstruction, we propose to perform these processes with FFT-based methods.

III. EVALUATING THE COEFFICIENTS USING THE FORWARD FFT

For a given 3D subsurface model, we propose to evaluate the coefficients of the Fourier series using the FFT.

In the Fourier series shown in (2), each Fourier term is a multiplication of cosine and sine functions. Since in a 1D Fourier transform spectrum, the real part and the imaginary part of a

frequency component are the cosine and sine functions respectively, we propose to use a series of 1D Fourier transforms to determine the coefficients of the 3D Fourier series to parameterize a 3D model.

We justify this statement with the following two arguments:

1) The multiple-dimensional Fourier transform can be implemented as several successive 1D Fourier transforms in sequence. Since this scheme is based on Fourier transforms, the accuracy of the model parameterization is guaranteed.

2) Each of the 1D Fourier transforms can be implemented in a fast way, called FFT. Therefore, this method can achieve high efficiency when applied to the 3D seismic inversion.

The determination of the truncated Fourier series coefficients can be described in the following three steps.

The first step is to perform 1D Fourier transform with respect to the z direction of the 3D model:

$$\mathcal{F}[u(r\Delta z)] = U_R(n\Delta k_z) - jU_I(n\Delta k_z) , \qquad (5)$$

for $r = 0,1,2,\cdots,N_z-1$, and $n = 0,1,2,\cdots,N_z-1$, where $u(r\Delta z)$ is referred to a 1D real signal, $j = \sqrt{-1}$ is the imaginary symbol, and separating each complex-valued Fourier component into two parts,

$$U_R(n\Delta k_z) = \sum_{r=0}^{N_z-1} u(r\Delta z)\cos(n\Delta k_z r),$$
$$U_I(n\Delta k_z) = \sum_{r=0}^{N_z-1} u(r\Delta z)\sin(n\Delta k_z r), \qquad (6)$$

the real part $U_R(n\Delta k_z)$ is a cosine transform, and the imaginary part $U_I(n\Delta k_z)$ is a sine transform. Implementation over the entire 3D volume will generate two 3D volumes $U_R(p\Delta x, q\Delta y, n\Delta k_z)$ and $U_I(p\Delta x, q\Delta y, n\Delta k_z)$.

The second step is, in a similar way, to perform 1D Fourier transform of two 3D volumes { $U_R(p\Delta x, q\Delta y, n\Delta k_z)$, $U_I(p\Delta x, q\Delta y, n\Delta k_z)$ } with respect to y as

$$\mathcal{F}[U_R(p\Delta x, q\Delta y, n\Delta k_z)] = U_{RR}(p\Delta x, m\Delta k_y, n\Delta k_z)$$
$$- jU_{IR}(p\Delta x, m\Delta k_y, n\Delta k_z),$$
$$\mathcal{F}[U_I(p\Delta x, q\Delta y, n\Delta k_z)] = U_{RI}(p\Delta x, m\Delta k_y, n\Delta k_z)$$
$$- jU_{II}(p\Delta x, m\Delta k_y, n\Delta k_z), \qquad (7)$$

resulting in four 3D volumes in the (x, k_y, k_z) domain: { $U_{RR}(p\Delta x, m\Delta k_y, n\Delta k_z)$, $U_{IR}(p\Delta x, m\Delta k_y, n\Delta k_z)$, $U_{RI}(p\Delta x, m\Delta k_y, n\Delta k_z)$, $U_{II}(p\Delta x, m\Delta k_y, n\Delta k_z)$ }.

The third step is, once again, to perform 1D Fourier transform of the four 3D volumes with respect to x,

$$\mathcal{F}[U_{RR}(p\Delta x, m\Delta k_y, n\Delta k_z)] = U_{RRR}(l\Delta k_x, m\Delta k_y, n\Delta k_z)$$
$$- jU_{IRR}(l\Delta k_x, m\Delta k_y, n\Delta k_z),$$
$$\mathcal{F}[U_{IR}(p\Delta x, m\Delta k_y, n\Delta k_z)] = U_{RIR}(l\Delta k_x, m\Delta k_y, n\Delta k_z)$$
$$- jU_{IIR}(l\Delta k_x, m\Delta k_y, n\Delta k_z),$$
$$\mathcal{F}[U_{RI}(p\Delta x, m\Delta k_y, n\Delta k_z)] = U_{RRI}(l\Delta k_x, m\Delta k_y, n\Delta k_z)$$
$$- jU_{IRI}(l\Delta k_x, m\Delta k_y, n\Delta k_z),$$
$$\mathcal{F}[U_{II}(p\Delta x, m\Delta k_y, n\Delta k_z)] = U_{RII}(l\Delta k_x, m\Delta k_y, n\Delta k_z)$$
$$- jU_{III}(l\Delta k_x, m\Delta k_y, n\Delta k_z), \qquad (8)$$

which result in eight 3D volumes in the (k_x, k_y, k_z) domain. Explicitly, they are

$$U_{RRR} = \sum_{(p,q,r)=(0,0,0)}^{(N_x-1,N_y-1,N_z-1)} u(p,q,r)\cos(l\Delta k_x p)\cos(m\Delta k_y q)\cos(n\Delta k_z r),$$

$$U_{IRR} = \sum_{(p,q,r)=(0,0,0)}^{(N_x-1,N_y-1,N_z-1)} u(p,q,r)\sin(l\Delta k_x p)\cos(m\Delta k_y q)\cos(n\Delta k_z r),$$

$$U_{RIR} = \sum_{(p,q,r)=(0,0,0)}^{(N_x-1,N_y-1,N_z-1)} u(p,q,r)\cos(l\Delta k_x p)\sin(m\Delta k_y q)\cos(n\Delta k_z r),$$

$$U_{IIR} = \sum_{(p,q,r)=(0,0,0)}^{(N_x-1,N_y-1,N_z-1)} u(p,q,r)\sin(l\Delta k_x p)\sin(m\Delta k_y q)\cos(n\Delta k_z r),$$

$$U_{RRI} = \sum_{(p,q,r)=(0,0,0)}^{(N_x-1,N_y-1,N_z-1)} u(p,q,r)\cos(l\Delta k_x p)\cos(m\Delta k_y q)\sin(n\Delta k_z r),$$

$$U_{IRI} = \sum_{(p,q,r)=(0,0,0)}^{(N_x-1,N_y-1,N_z-1)} u(p,q,r)\sin(l\Delta k_x p)\cos(m\Delta k_y q)\sin(n\Delta k_z r),$$

$$U_{RII} = \sum_{(p,q,r)=(0,0,0)}^{(N_x-1,N_y-1,N_z-1)} u(p,q,r)\cos(l\Delta k_x p)\sin(m\Delta k_y q)\sin(n\Delta k_z r),$$

$$U_{III} = \sum_{(p,q,r)=(0,0,0)}^{(N_x-1,N_y-1,N_z-1)} u(p,q,r)\sin(l\Delta k_x p)\sin(m\Delta k_y q)\sin(n\Delta k_z r), \qquad (9)$$

where $U_{RRR} \equiv U_{RRR}(l\Delta k_x, m\Delta k_y, n\Delta k_z)$ and so on. The procedure is summarized in Fig. 1. The 1D Fourier transforms in this study are implemented using the free software library Fastest Fourier Transform in the West (FFTW), which computes the discrete Fourier transform (DFT) [13].

Comparing (9) with the Fourier coefficients formulas presented in (A-1) to (A-6), the coefficients of the Fourier series may be evaluated through those Fourier transform components as

$$\begin{aligned}
a_{lmn} &= \beta_{lmn}U_{RRR}, & b_{lmn} &= \beta_{lmn}U_{IRR}, \\
c_{lmn} &= \beta_{lmn}U_{RIR}, & d_{lmn} &= \beta_{lmn}U_{IIR}, \\
e_{lmn} &= \beta_{lmn}U_{RRI}, & f_{lmn} &= \beta_{lmn}U_{IRI}, \\
g_{lmn} &= \beta_{lmn}U_{RII}, & h_{lmn} &= \beta_{lmn}U_{III},
\end{aligned} \qquad (10)$$

where

$$\beta_{lmn} = \begin{cases} 8\alpha, & \text{for } (l,m,n) > 0, \\ 4\alpha, & \text{for } \begin{cases} (l,m > 0, n = 0), \\ (l, n > 0, m = 0), \\ (m, n > 0, l = 0), \end{cases} \\ 2\alpha, & \text{for } \begin{cases} (l > 0, m = n = 0), \\ (m > 0, l = n = 0), \\ (n > 0, l = m = 0), \end{cases} \\ \alpha, & \text{for } (l = m = n = 0). \end{cases} \quad (11)$$

and

$$\alpha = \frac{1}{N_x N_y N_z}. \quad (12)$$

Equations (10)-(12) explicitly show that the Fourier transform components after three times Fourier transform are not equal to the Fourier coefficients of the truncated Fourier series. They are connected by (10).
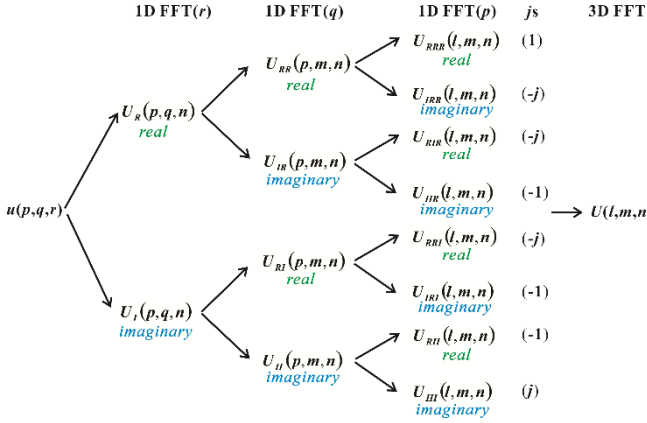

Fig. 1. Relationship between three times 1D FFT along three directions and 3D FFT.

In this study, the estimation of Fourier coefficients using (A-1) to (A-6) and (9) to (12) is defined as direct forward Fourier series method and forward FFT-based method, respectively.

IV. RECONSTRUCTING THE 3D MODEL BY THE INVERSE FFT

We propose to reconstruct the 3D model by the inverse FFT at each iteration of the inversion procedure once the truncated Fourier series from the inversion has been obtained. This inverse FFT-based scheme significantly improves efficiency compared to the conventional direct calculation with (1).

As shown in Fig. 1, the complex-valued 3D volume is formed by the eight Fourier components as follows:

$$U = U_{RRR} - U_{IIR} - U_{IRI} - U_{RII} \\ - j[U_{IRR} + U_{RIR} + U_{RRI} - U_{III}]. \quad (13)$$

This complex-valued 3D volume $U \equiv U(l,m,n)$ is input to an inverse 3D FFT to reconstruct a 3D model in the spatial domain. In the following section, we will prove that the 3D inverse FFT of U is a special case of (1).

Implementing a 3D inverse FFT to U, one may have

$$u(p,q,r) = \alpha \sum_{(l,m,n)=(0,0,0)}^{(N_x-1, N_y-1, N_z-1)} \Psi_{lmn}(p,q,r), \quad (14)$$

where

$$\begin{aligned} \Psi_{lmn}&(p,q,r) \\ =& U_{RRR} \cos(l\Delta k_x p)\cos(m\Delta k_y q)\cos(n\Delta k_z r) \\ +& U_{IRR} \sin(l\Delta k_x p)\cos(m\Delta k_y q)\cos(n\Delta k_z r) \\ +& U_{RIR} \cos(l\Delta k_x p)\sin(m\Delta k_y q)\cos(n\Delta k_z r) \\ +& U_{IIR} \sin(l\Delta k_x p)\sin(m\Delta k_y q)\cos(n\Delta k_z r) \\ +& U_{RRI} \cos(l\Delta k_x p)\cos(m\Delta k_y q)\sin(n\Delta k_z r) \\ +& U_{IRI} \sin(l\Delta k_x p)\cos(m\Delta k_y q)\sin(n\Delta k_z r) \\ +& U_{RII} \cos(l\Delta k_x p)\sin(m\Delta k_y q)\sin(n\Delta k_z r) \\ +& U_{III} \sin(l\Delta k_x p)\sin(m\Delta k_y q)\sin(n\Delta k_z r). \end{aligned} \quad (15)$$

Considering the original 3D model is real-valued, the complex conjugate symmetry is exploited. As described in the previous section, the three 1D DFTs are implemented in the sequence of $z \rightarrow y \rightarrow x$. Based on the complex conjugate property, when $l > 0$, we can get the values of $U_{RRR}, U_{IIR}, \cdots, U_{III}$ at $(N_x - l, m, n)$ from their counterparts at (l,m,n). When the three 1D DFTs are implemented in the sequence of $z \rightarrow x \rightarrow y$, in a similar way, we can deduce the values at $(l, N_y - m, n)$ and $(N_x - l, N_y - m, n)$ from the counterparts at (l,m,n) and $(N_x - l, m, n)$. Similarly, when the three 1D DFTs are implemented in the sequence of $x \rightarrow y \rightarrow z$, we can obtain values at $(l, m, N_z - n)$, $(N_x - l, m, N_z - n)$, $(l, N_y - m, N_z - n)$ and $(N_x - l, N_y - m, N_z - n)$ from those at (l,m,n), $(N_x - l, m, n)$, $(l, N_y - m, n)$ and $(N_x - l, N_y - m, n)$, respectively. Using the relations between the three sequences, the conjugate components of $U_{RRR}, U_{IRR}, \cdots, U_{III}$ are listed in Table 1, and Table 2 lists the constants c_1, c_2, ..., c_8, needed in Table 1. The zero-valued constants mean there are zero values in l, m, n and its conjugate counterpart does not exist.

Substituting $U_{RRR}, U_{IRR}, \cdots, U_{III}$ in Table 1 into (15), when $l, m, n > 0$, one may have

$$\begin{aligned} \Psi(l,m,n) &= \Psi(N_x - l, m, n) = \Psi(l, N_y - m, n) \\ &= \Psi(N_x - l, N_y - m, n) = \Psi(l, m, N_z - n) \\ &= \Psi(N_x - l, m, N_z - n) = \Psi(l, N_y - m, N_z - n) \\ &= \Psi(N_x - l, N_y - m, N_z - n), \end{aligned} \quad (16)$$

and set $\gamma(l,m,n) = 8$. In the same way, $\gamma(l,m,n) = 4, 2, 1$ when there are one, two and three zeros in (l,m,n). The values of $\gamma(l,m,n)$ are also listed in Table 2. Therefore, (14) can be rewritten as

$$u(p,q,r) = \alpha \sum_{(l,m,n)=(0,0,0)}^{(N_x/2, N_y/2, N_z/2)} \gamma_{lmn} \Psi_{lmn}(p,q,r), \quad (17)$$

From (10) and (11), (17) is equivalent to

$$u(p,q,r) = \sum_{(l,m,n)=(0,0,0)}^{(N_x/2,N_y/2,N_z/2)} \varphi_{lmn}(p,q,r). \qquad (18)$$

Equation (18) shows that if $L = N_x/2 + 1, M = N_y/2 + 1$, $N = N_z/2 + 1$, the model can be completely reconstructed from the Fourier coefficients. This also means that (1) can be realised by an inverse 3D DFT. However, we cannot use the Fourier coefficients directly to implement the inverse DFT, but we must first reconstruct $U(l,m,n)$ from the Fourier coefficients. Since the Fourier series is truncated, (L, M, N) is

smaller than $(N_x/2+1, N_y/2+1, N_z/2+1)$. Therefore, in the construction of $U(l,m,n)$, the unestimated Fourier coefficients are set to zero. For the estimated Fourier coefficients, the corresponding $U_{RRR}, U_{IRR}, \cdots, U_{III}$ are available from (10), and the conjugate counterparts can be calculated using Tables 1 and 2. When $U(l,m,n)$ is prepared, the 3D model is reconstructed after implementing an inverse 3D FFT.

TABLE 1
THE REAL AND IMAGINARY COMPONENTS CONJUGATE TO
$(l,m,n), l \in [0, N_x - 1], m \in [0, N_y - 1], n \in [0, N_z - 1]$.

	(l,m,n)	$(N_x - l, m, n)$	$(l, N_y - m, n)$	$(N_x - l, N_y - m, n)$
$(U_{RRR}^{ijk}, U_{IRR}^{ijk})$	$c_1(U_{RRR}^{lmn}, U_{IRR}^{lmn})$	$c_2(U_{RRR}^{lmn}, -U_{IRR}^{lmn})$	$c_3(U_{RRR}^{lmn}, U_{IRR}^{lmn})$	$c_4(U_{RRR}^{lmn}, -U_{IRR}^{lmn})$
$(U_{RIR}^{ijk}, U_{IIR}^{ijk})$	$c_1(U_{RIR}^{lmn}, U_{IIR}^{lmn})$	$c_2(U_{RIR}^{lmn}, -U_{IIR}^{lmn})$	$c_3(-U_{RIR}^{lmn}, -U_{IIR}^{lmn})$	$c_4(-U_{RIR}^{lmn}, U_{IIR}^{lmn})$
$(U_{RRI}^{ijk}, U_{IRI}^{ijk})$	$c_1(U_{RRI}^{lmn}, U_{IRI}^{lmn})$	$c_2(U_{RRI}^{lmn}, -U_{IRI}^{lmn})$	$c_3(U_{RRI}^{lmn}, U_{IRI}^{lmn})$	$c_4(U_{RRI}^{lmn}, -U_{IRI}^{lmn})$
$(U_{RII}^{ijk}, U_{III}^{ijk})$	$c_1(U_{RII}^{lmn}, U_{III}^{lmn})$	$c_2(U_{RII}^{lmn}, -U_{III}^{lmn})$	$c_3(-U_{RII}^{lmn}, -U_{III}^{lmn})$	$c_4(-U_{RII}^{lmn}, U_{III}^{lmn})$

	$(l,m,N_z - n)$	$(N_x - l, m, N_z - n)$	$(l, N_y - m, N_z - n)$	$(N_x - l, N_y - m, N_z - n)$
$(U_{RRR}^{ijk}, U_{IRR}^{ijk})$	$c_5(U_{RRR}^{lmn}, U_{IRR}^{lmn})$	$c_6(U_{RRR}^{lmn}, -U_{IRR}^{lmn})$	$c_7(U_{RRR}^{lmn}, U_{IRR}^{lmn})$	$c_8(U_{RRR}^{lmn}, -U_{IRR}^{lmn})$
$(U_{RIR}^{ijk}, U_{IIR}^{ijk})$	$c_5(U_{RIR}^{lmn}, U_{IIR}^{lmn})$	$c_6(U_{RIR}^{lmn}, -U_{IIR}^{lmn})$	$c_7(-U_{RIR}^{lmn}, -U_{IIR}^{lmn})$	$c_8(-U_{RIR}^{lmn}, U_{IIR}^{lmn})$
$(U_{RRI}^{ijk}, U_{IRI}^{ijk})$	$c_5(-U_{RRI}^{lmn}, -U_{IRI}^{lmn})$	$c_6(-U_{RRI}^{lmn}, U_{IRI}^{lmn})$	$c_7(-U_{RRI}^{lmn}, -U_{IRI}^{lmn})$	$c_8(-U_{RRI}^{lmn}, U_{IRI}^{lmn})$
$(U_{RII}^{ijk}, U_{III}^{ijk})$	$c_5(-U_{RII}^{lmn}, -U_{III}^{lmn})$	$c_6(-U_{RII}^{lmn}, U_{III}^{lmn})$	$c_7(U_{RII}^{lmn}, U_{III}^{lmn})$	$c_8(U_{RII}^{lmn}, -U_{III}^{lmn})$

TABLE 2
THE c VALUES FOR THE COMPLEX COUNTERPARTS IN THE CONJUGATE POSITIONS

	c_1	c_2	c_3	c_4	c_5	c_6	c_7	c_8	γ_{lmn}
$l,m,n>0$	1	1	1	1	1	1	1	1	8
$l=0,m,n>0$	1	0	1	0	1	0	1	0	4
$m=0,l,n>0$	1	1	0	0	1	1	0	0	4
$n=0,l,m>0$	1	1	1	1	0	0	0	0	4
$l>0,m=n=0$	1	1	0	0	0	0	0	0	2
$m>0,l=n=0$	1	0	1	0	0	0	0	0	2
$n>0,l=m=0$	1	0	0	0	1	0	0	0	2
$l=m=n=0$	1	0	0	0	0	0	0	0	1

In summary, the procedure for constructing the 3D model from the coefficients of the truncated Fourier series consists of the following five steps:

1) Calculating $U_{RRR}, U_{IRR}, \cdots, U_{III}$ from the Fourier coefficients according to (10)-(12);
2) Calculating the conjugate components according to Tables 1 and 2;
3) Set the remaining values of $U_{RRR}, U_{IRR}, \cdots, U_{III}$ to 0;
4) Use (13) to calculate the complex series $U(l,m,n)$;
5) Apply an inverse 3D FFT to the 3D complex series $U(l,m,n)$; the resulting real-valued 3D volume is the 3D model.

In this study, the 3D inverse FFT is also realized by the 3D inverse DFT in FFTW, requiring only $N_x \times N_y \times (N_z/2+1)$ complex-valued $U(l,m,n)$ as input [13].

Similar to the estimation of the Fourier coefficients, the reconstruction of the model from the coefficients using (1) to (2) and the five-step procedure are called the inverse direct Fourier series method or inverse FFT-based method.

V. APPLICABILITY

Now, we test the applicability of this model parameterization scheme by using the forward and inverse FFT pair, for model fitting and model reconstruction.

A. Model fitting by a truncated Fourier series

Fig. 2a is a 3D overthrust impedance model, and Fig. 2b is the corresponding seismic data cube, generated by the wave equation simulation, with some missing traces. The model size is $N_x = N_y = 400$, and $N_z = 150$. In this example, N_x corresponds to the trace number in the x direction, ranging

from 0 to 399, N_y corresponds to the trace number in the y direction, varying from 0 to 399, and the vertical index N_z is the number of time samples, ranging from 0 s to 0.894 s with an interval of 6 ms.

The time needed to calculate the Fourier coefficients depends on the chosen values (L, M, N). Small values of (L, M, N) correspond to the low wavenumber components of the impedance model, while the large values of (L, M, N) correspond to the high wavenumber components. In this study, we compare four cases of (L, M, N): (5, 5, 5), (20, 20, 10), (40, 40, 20) and (201, 201, 76). The time costs of the FFT-based

method for these four cases are 0.15, 0.162, 0.163 and 0.178 minutes, respectively. They are almost the same because in each case we first implement a triple 1D FFT, and then calculate the Fourier coefficients using (10), which accounts for the time differences between the different cases. On the other hand, if we calculate the Fourier series directly, the time costs required for the corresponding four cases are 0.25, 8.03, 65 and 6164.2 minutes, respectively (Table 3). It is obvious that the FFT-based method is significantly faster than the direct Fourier series calculation.
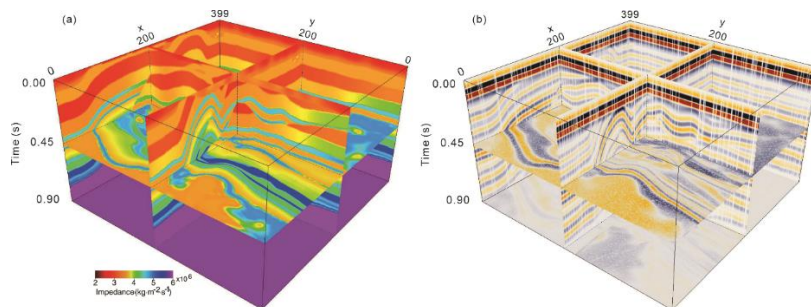

Fig. 2. (a) The 3D overthrust impedance model. (b) The synthetic seismic data with null traces, generated by wave equation simulation.
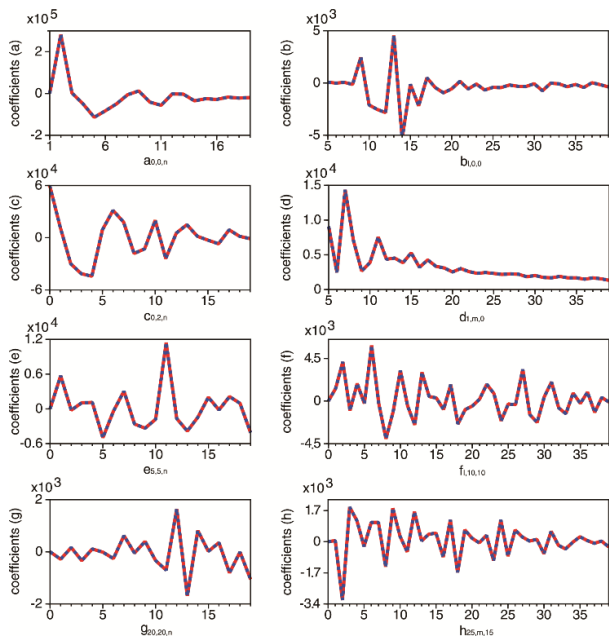

Fig. 3. Eight groups of coefficients selected from the Fourier coefficient cubes. The size of each cube is $40 \times 40 \times 20$, because the selected number of Fourier coefficients in each direction are (L, M, N) = (40, 40, 20). (a) is for coefficients a_{00n} with $l = m = 0, 1 \leq n < 20$. (b) is for b_{l00} with { $m = n = 0, 5 \leq l < 40$ }. $b_{l00} (0 \leq l < 5)$ is not included because it is much larger than $b_{l00} (5 \leq l < 40)$ by two orders of magnitudes, which may result in the latter unrecognized. The rest coefficients (c)-(h) are plotted in the same way. The red solid curves are from the direct Fourier series calculation. The blue dot curves are from the FFT-based method.
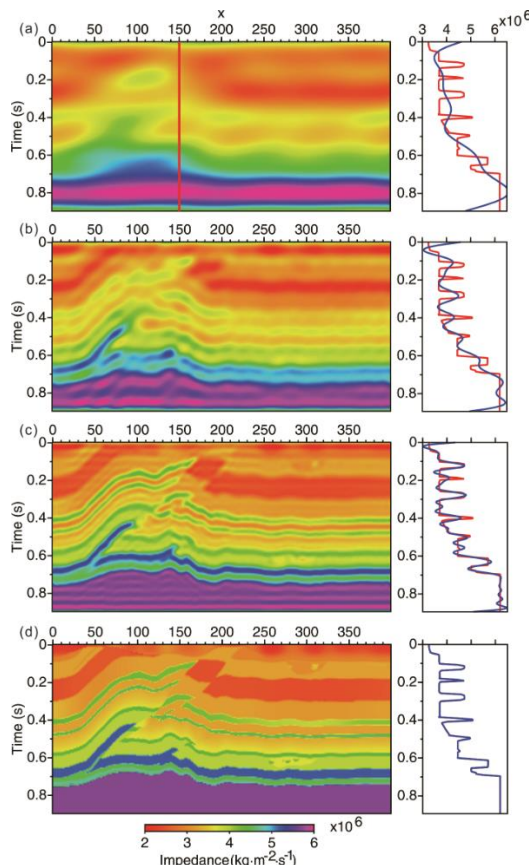

Fig. 4. The impedance models, located at y=250 from the 3D model, reconstructed from the truncated Fourier series with (L, M, N) equal to (5, 5, 5), (20, 20, 10), (40, 40, 20) and (201, 201, 76) from (a)-(d), respectively. The curves in the right side of (a-d) are the impedance traces at (x, y) = (150, 250). The red curves are extracted from the true impedance model, and the blue lines are from the reconstructed impedance model.

To verify the accuracy of the Fourier coefficients estimated by the FFT method, they are compared with the Fourier coefficients obtained by the forward direct Fourier series method. Since each of the coefficients $\{a_{lmn}, b_{lmn}, \cdots, h_{lmn}\}$ is a 3D cube with the size of $L \times M \times N$, we select only a small portion of the data from each Fourier coefficient for comparison. Fig. 3 shows eight groups of Fourier coefficients for $(L, M, N) = (40, 40, 20)$. Fig. 3a is for Fourier coefficients a_{00n} with $l = m = 0, 1 \le n < 20$ and Fig. 3b is for coefficients b_{l00} with $m = n = 0, 5 \le l < 40$. Fig. 3c-h are selected in the same way for the other Fourier coefficients. In Fig. 3, the red curves are estimated by direct Fourier series calculation, and the blue dotted curves are calculated by the FFT-based method. The results of the two methods are identical.

B. Model reconstruction from the Fourier coefficients

Fig. 4 compares the original impedance profile and the models reconstructed from the truncated Fourier series coefficients with $(L, M, N) = (5, 5, 5)$, $(20, 20, 10)$, $(40, 40, 20)$ and $(201, 201, 76)$. The reconstruction method based on the inverse FFT and the direct Fourier series construction method give identical results. Therefore, Fig. 4 shows only the result of the inverse FFT-based method. The sample profiles were taken at $y=250$. The impedance model constructed from Fourier coefficients with large values (L, M, N) is much closer to the true model. The relative errors of the four cases of (L, M, N) are 11.5%, 8.1%, 5.3% and 0.0% respectively. The errors decrease as the values of (L, M, N) increase. When $(L, M, N) = (201, 201, 76)$, the reconstructed impedance profile corresponds exactly the real model. When model parameterization with truncated Fourier series is applied to seismic inversion, we can increase the number of Fourier coefficients from small-valued (L, M, N) to large-valued (L, M, N), and thus gradually reconstruct the low- and high-wavenumber components of the subsurface model.

The right side of panel a–d in Fig. 4 compares the impedance traces at $(x, y) = (150, 250)$. The red curves are the true impedance model traces, and the blue curves are the reconstructed impedance traces. Fourier coefficients with small values (L, M, N) mainly give the background of the impedance model, while the large values (L, M, N) give a refined impedance model. When $(L, M, N) = (201, 201, 76)$, the red and blue curves overlap, which mean that the impedance model has been completely reconstructed from the Fourier coefficients.

Table 3 also lists the time cost of reconstructing the 3D model from the truncated Fourier series. The time costs for the inverse direct Fourier series method, where the model is reconstructed using (1), are 0.24, 7.23, 57.9 and 5550 minutes for the four (L, M, N)s, respectively. The time required for the inverse FFT-based method is almost the same, about 0.02 minutes for the four cases, and the slight differences are due to the preparation of the complex series $U(l, m, n)$. Therefore, the inverse FFT-based method can reconstruct the impedance model from the truncated Fourier series very fast, which makes the 3D seismic inversion for impedance efficient and

time saving when this model parameterization scheme is applied.

VI. APPLICATION IN SEISMIC IMPEDANCE INVERSION

A. The inversion theory

In this section, model parameterization with truncated Fourier coefficients is applied to 3D seismic impedance inversion from migrated seismic data. The inversion is performed using wave equation theory. The equation is expressed as follows (Wang, 2016):

$$4\frac{\partial}{\partial \tau}\left(\sigma(\tau)\frac{\partial w(\tau,t)}{\partial \tau}\right) - \sigma(\tau)\frac{\partial^2 w(\tau,t)}{\partial t^2} = 0, \quad (19)$$

where $\sigma(\tau)$ is the impedance in the depth-time domain, τ is the depth-time, w is the wavefield, and t is the travelling time.

Equation (19) is obtained by transforming the traditional 1D wave equation from the depth domain to the depth-time domain. Then the traditional wave equation with two parameters defined by velocity and density becomes a wave equation with one parameter, impedance. In this test, the waveform inversion method [14], [15], [16] is used to invert the impedance from a single seismic trace.

To invert a 3D impedance model from the seismic cube, we combine the 1D impedance inversion with the truncated Fourier series. By fitting the 3D impedance model with a truncated Fourier series, the impedance inversion problem is transformed into the problem of first inverting the Fourier coefficients, and then reconstructing the 3D impedance model from the inverted Fourier coefficients. In the inversion for Fourier coefficients, the misfit function is defined as

$$\phi(\mathbf{m}) = \frac{1}{2}\iiint_{x,y,t}\left[\mathbf{w}_{obs}(x,y,t) - \mathbf{w}_{syn}(x,y,t,\mathbf{m})\right]^2 \mathrm{d}x\mathrm{d}y\mathrm{d}t, \quad (20)$$

where $\mathbf{w}_{obs}(x,y,t)$ is the observed waveforms and $\mathbf{w}_{syn}(x,y,t,\mathbf{m})$ is the synthetic waveforms generated from the model.

The gradient with respect to the Fourier coefficients, such as d_{lmn}, is derived as

$$\frac{\partial \phi(\mathbf{m})}{\partial d_{lmn}} = -\iiiint_{x\ y\ z\ t}\frac{\partial \sigma(x,y,z)}{\partial d_{lmn}}\frac{\partial \mathbf{w}_{syn}(x,y,t,\mathbf{m})}{\partial \sigma(x,y,z)} \quad (21)$$
$$\times \left[\mathbf{w}_{obs}(x,y,t) - \mathbf{w}_{syn}(x,y,t,\mathbf{m})\right]\mathrm{d}t\mathrm{d}z\mathrm{d}y\mathrm{d}x.$$

It can be seen from (21) that the chain rule is followed to obtain the gradients with respect to d_{lmn}, and this procedure involves three steps. The first step is to calculate the gradients with respect to the impedance at the (x, y)th trace by correlation between the forward and backward wavefields. In the second step, the gradients at the (x, y)-th trace are used to calculate the gradient with respect to d_{lmn}. By parameterizing the impedance with the truncated Fourier series, the gradient of the impedance is

$$\frac{\partial \sigma(x,y,z)}{\partial d_{lmn}} = \sin(l\Delta k_x p)\sin(m\Delta k_y q)\cos(n\Delta k_z r), \quad (22)$$

where $x = p\Delta x, y = q\Delta y, z = r\Delta z$. After finishing the second step, the final step is to sum up the gradients to d_{lmn} in all traces.

B. The inversion strategies

In the inversion of Fourier coefficients, the starting evaluation of Fourier coefficients is determined from the 3D initial impedance model with the forward FFT-based method, and then the Fourier coefficients are inverted with increasing number in (L, M, N). The number of (L, M, N)s increases from small to large values. Using the Fourier coefficients with the numbers of (L, M, N), the corresponding 3D impedance model can be reconstructed very fast using the inverse FFT-based method, which is used to calculate the gradients in the next iteration.

For updating Fourier coefficients with each (L, M, N), only several subsets of seismic traces are involved. This is because the impedance at each position and time is a function of the Fourier coefficients, as can be seen from (1) and (2). Therefore, impedance traces inverted from one part of the seismic cube may be sufficient to update the Fourier coefficients, avoiding redundancy and saving computational

time. If the seismic traces in a subgroup are selected for example, every 5 traces, in both the x and y directions from the seismic cube, a total of 25 subgroups are generated, which are $D_{s,t}^{(5)}, 1 \le s, t \le 5$. The first data subgroup can be explicitly expressed as follows:

$$D_{1,1}^{(5)} = \left\{ \begin{array}{ccccc} \mathbf{w}_{0,0} & \mathbf{w}_{0,1} & \cdots & \mathbf{w}_{0,396} & \mathbf{w}_{0,399} \\ \mathbf{w}_{1,0} & \mathbf{w}_{1,1} & \cdots & \mathbf{w}_{1,396} & \mathbf{w}_{1,399} \\ \vdots & \vdots & \ddots & \vdots & \vdots \\ \mathbf{w}_{396,0} & \mathbf{w}_{396,1} & \cdots & \mathbf{w}_{396,396} & \mathbf{w}_{396,399} \\ \mathbf{w}_{399,0} & \mathbf{w}_{399,1} & \cdots & \mathbf{w}_{399,396} & \mathbf{w}_{399,399} \end{array} \right\}, \quad (23)$$

where $\mathbf{w}_{p,q}$ is seismic trace at the pth and qth position, 5 is the trace interval for subgroup selection, and the subscript of $D_{1,1}^{(5)}$ is equal to the subscript of $\mathbf{w}_{1,1}$, representing the position of the first trace selected that satisfies $0 < p, q < 399$. The traces { $\mathbf{w}_{0,q}, \mathbf{w}_{p,0}, \mathbf{w}_{399,q}, \mathbf{w}_{p,399}$ } are included in each subgroup to satisfy the periodic condition of the Fourier series [6]. The traces in the remaining 24 subgroups are selected in the same way. In the inversion of Fourier coefficients, we can only use some subgroups.

TABLE 3
THE COMPUTATION COST(MINS) FOR EVALUATING THE COEFFICIENTS
AND FOR RECONSTRUCTING 3D MODEL

	(L,M,N)	(5,5,5)	(20,20,10)	(40,40,20)	(201,201,76)
Evaluating the Fourier series from a 3D model (mins)	Forward direct Fourier series method	0.25	8.03	65	6164.2
	Forward FFT-based method	0.15	0.162	0.163	0.178
Reconstructing 3D model from the Fourier series (mins)	Inverse direct Fourier series method	0.24	7.23	57.9	5550
	Inverse FFT-based method	0.02	0.02	0.02	0.03

To demonstrate the feasibility of model parameterization and inversion strategies in 3D seismic impedance inversion, both examples of a synthetic overthrust model and a test with field data are presented. In the following sections, the impedance inversion with model parameterization using truncated Fourier series coefficients is referred to as the Fourier coefficient-based method.

C. Synthetic overthrust model example

In the impedance inversion of the 3D overthrust model, as shown in Fig. 2a, we compare the inversion results of the trace-by-trace method, and the Fourier coefficient-based method, which uses a seismic cube with missing traces. Fig. 2b shows the corresponding synthetic seismic cube, generated using (19). The source for this synthetic data is a Ricker wavelet with a main frequency of 10 Hz. In Fig. 2b, 25011 null traces are randomly distributed in the cube, which contains a total of 160000 traces.

Fig. 5a shows two cross profiles of the overthrust impedance model at x=100 and y=100 (Fig. 2a). Fig. 5b is the initial impedance profile for the inversion, smoothed with a

3D smoothing function from the real model. We chose Fig. 5b as the initial model because both the trace-by-trace method and the Fourier coefficient-based method are local optimization methods. In the Fourier coefficient-based method, the 1D inversion procedure is a local optimization process that determines the dependence on the initial model, while the model parameterization with truncated Fourier series mainly aims at reducing the number of inverted parameters, preserving spatial continuity, and improving robustness, which will be demonstrated in the following sections.

Fig. 5c shows the inverted impedance profiles using the trace-by-trace method, in which the impedance traces are not recovered at positions with null seismic trace. In this inversion, 40 threads ($NPRO = 40$) are used for parallel execution and 10 iterations are set as the maximum iterations. It takes 4 minutes to complete the inversion of 134989 seismic traces, excluding the null traces, on a workstation with 48 cores and 96 threads.

In the Fourier coefficient-based method, the initial Fourier coefficients with $L = 201, M = 201, N = 76$ are estimated using the forward FFT-based method from the initial

impedance model. In this test, every 5 traces in the x and y directions are selected from the seismic cube to form a subgroup. Table 4 shows the subgroups used for each (L, M, N), where 19/25 of the subgroups are used to update the Fourier coefficients.

In the first inversion stage, the inversion begins with (L, M, N) = (20, 20, 10), which is approximately one-tenth of $\left(N_x/2+1, N_y/2+1, N_z/2+1\right)$. In this stage, the inversion is performed for a small number of Fourier coefficients, which corresponds to the inversion of low-wavenumber components of the impedance model. Fig. 6a shows the inverted impedance profiles of the first stage. The inversion increases the values of (L, M, N) stepwise with a step size of (20, 20, 10), which is usually fixed at 1~2 times the initial values of (L, M, N). Fig. 6b is the result of the second step, when (L, M, N) = (40, 40, 20). Fig. 6c-d are the results of the inversion in the third and final stage when (L, M, N) = (60, 60, 30) and (80, 80, 40), respectively. Compared to the trace-by-trace method, the inverted impedance profiles are spatially continuous, even if there are null traces in the seismic cube, and they are also close to the true model profiles. Note that the total number of Fourier coefficients in the last stage is $8 \times 80 \times 80 \times 40$, which is less than the total number of impedance ($400 \times 400 \times 150$).

We also compare the inverted seismic impedance slices with the real model. Fig. 7 shows slices at times 0.24 s, 0.45 s and 0.66 s. The comparison shows that the inverted 3D impedance model agrees well with to the real model.

When testing the Fourier coefficient-based method, we use the same number (40) of threads to for the parallel implementation, as for the trace-by-trace method. The time required is 21.5 minutes, with the computation time for the four groups of (L, M, N) being about 0.5, 2.0, 5.0, and 14.0 minutes, respectively. It is clear that Fourier coefficients with large values (L, M, N) require more computation time for updating. Since the model reconstruction is fast and its time cost is almost independent of (L, M, N), the calculation of the gradient to the Fourier coefficients and the seismic traces used for inversion are responsible for the increasing computation time. From Fig. 6, it can be seen that the reconstructed model profiles from the inverted Fourier coefficients with large values (L, M, N) are closer to the true model profiles. The inversion procedure stops when (L, M, N) reaches the maximum values of (L, M, N) or the relative errors, between the synthetic and the observed data or between the models from Fourier coefficients of two adjacent (L, M, N) meet a threshold.

When testing the Fourier coefficient-based method, we use the same number (40) of threads to for the parallel implementation, as for the trace-by-trace method. The time required is 21.5 minutes, with the computation time for the four groups of (L, M, N) being about 0.5, 2.0, 5.0, and 14.0 minutes, respectively. It is clear that Fourier coefficients with large values (L, M, N) require more computation time for updating. Since the model reconstruction is fast and its time cost is almost independent of (L, M, N), the calculation of the gradient to the Fourier coefficients and the seismic traces used for inversion are responsible for the increasing computation time. From Fig. 6, it can be seen that the reconstructed model profiles from the inverted Fourier coefficients with large values (L, M, N) are closer to the true model profiles. The inversion procedure stops when (L, M, N) reaches the maximum values of (L, M, N) or the relative errors, between the synthetic and the observed data or between the models from Fourier coefficients of two adjacent (L, M, N) meet a threshold.

We also compare the inverted seismic impedance slices with the real model. Fig. 7 shows slices at times 0.24 s, 0.45 s and 0.66 s. The comparison shows that the inverted 3D impedance model agrees well with to the real model.

TABLE 4
SUB-DATA GROUPS USED FOR THE IMPEDANCE INVERSION WITH DIFFERENT TRACES SELECTION INTERVALS (5 AND 10)

| (L,M,N)	Sub-data groups used for the impedance inversion
(20,20,10)	$\left\{ D_{1,1}^{(5)}, D_{1,5}^{(5)}, D_{5,1}^{(5)}, D_{5,5}^{(5)} \right\}$
	$\left\{ D_{1,1}^{(10)}, D_{1,5}^{(10)}, D_{1,9}^{(10)}, D_{5,1}^{(10)}, D_{5,5}^{(10)}, D_{5,9}^{(10)}, D_{9,1}^{(10)}, D_{9,5}^{(10)}, D_{9,9}^{(10)} \right\}$
(40,40,20)	$\left\{ D_{1,1}^{(5)}, D_{1,3}^{(5)}, D_{1,5}^{(5)}, D_{3,1}^{(5)}, D_{3,3}^{(5)}, D_{3,5}^{(5)}, D_{5,1}^{(5)}, D_{5,3}^{(5)}, D_{5,5}^{(5)} \right\}$
	$\left\{ D_{1,2}^{(10)}, D_{1,5}^{(10)}, D_{1,8}^{(10)}, D_{4,2}^{(10)}, D_{4,5}^{(10)}, D_{4,8}^{(10)}, D_{7,2}^{(10)}, D_{7,5}^{(10)}, D_{7,8}^{(10)}, D_{10,2}^{(10)}, D_{10,5}^{(10)}, D_{10,8}^{(10)} \right\}$
(60,60,30)	$\left\{ D_{2,3}^{(5)}, D_{2,4}^{(5)}, D_{2,5}^{(5)}, D_{5,3}^{(5)}, D_{5,4}^{(5)}, D_{5,5}^{(5)} \right\}$
	$\left\{ D_{4,3}^{(10)}, D_{4,6}^{(10)}, D_{4,9}^{(10)}, D_{7,3}^{(10)}, D_{7,6}^{(10)}, D_{7,9}^{(10)}, D_{10,3}^{(10)}, D_{10,6}^{(10)}, D_{10,9}^{(10)} \right\}$
(80,80,40)	$\left\{ D_{2,2}^{(5)}, D_{2,4}^{(5)}, D_{3,2}^{(5)}, D_{3,4}^{(5)}, D_{4,2}^{(5)}, D_{4,4}^{(5)}, D_{5,2}^{(5)}, D_{5,4}^{(5)} \right\}$
	$\left\{ D_{2,2}^{(10)}, D_{2,5}^{(10)}, D_{2,8}^{(10)}, D_{5,2}^{(10)}, D_{5,5}^{(10)}, D_{5,8}^{(10)}, D_{8,2}^{(10)}, D_{8,5}^{(10)}, D_{8,8}^{(10)} \right\}$
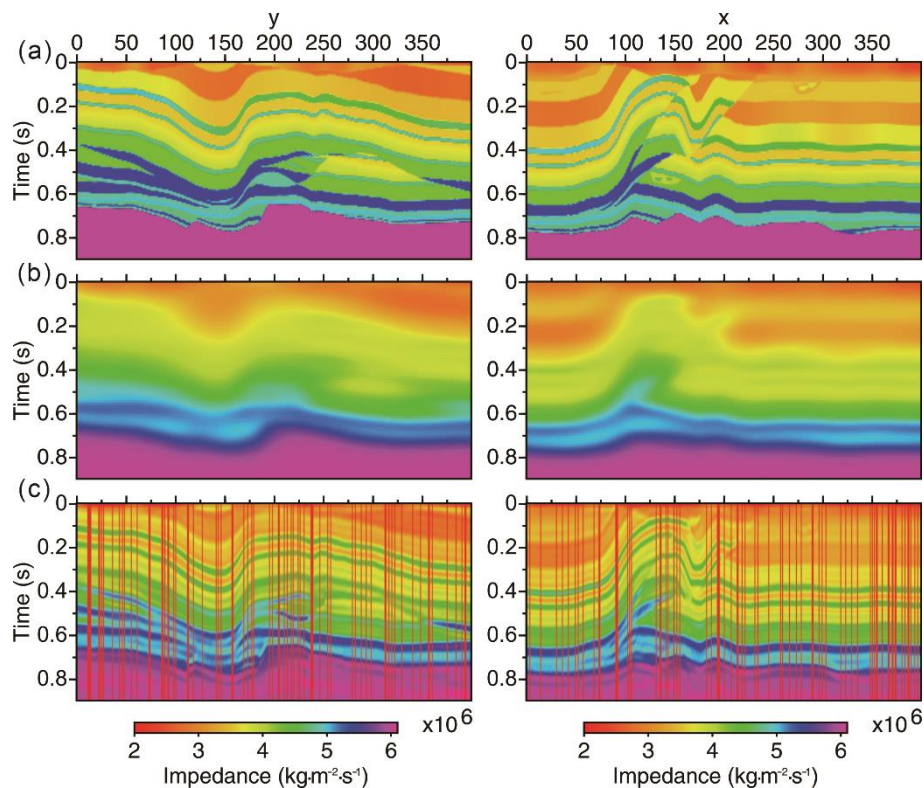
Fig. 5. (a) The true impedance profiles. (b) The initial impedance profiles set for the inversion. (c) The inverted impedance profiles obtained by the trace-by-trace inversion method. The left and right panels of each subfigures are impedance profiles at x=100 and y=100, respectively.

Here we show how the seismic traces affect the inversion results and the computation time by the inversion results when the subgroup is selected by every 10 traces in the x and y directions. The subgroups used in each case are listed in Table 4, with 37/100 of the total subgroups included. The other parameters are the same as those in the case of intervals with 5. The inversion takes about 10 minutes. The inverted

impedance profiles at x=100 and y=100 are shown in Fig. 8. Compared to Fig. 6d, it can be seen that some spatial discontinuities have occurred in the profiles, indicated by the red circles. Therefore, we have to make a trade-off between spatial continuity and computation time. A coverage of more than 70% of the total subgroups can lead to continuous results.
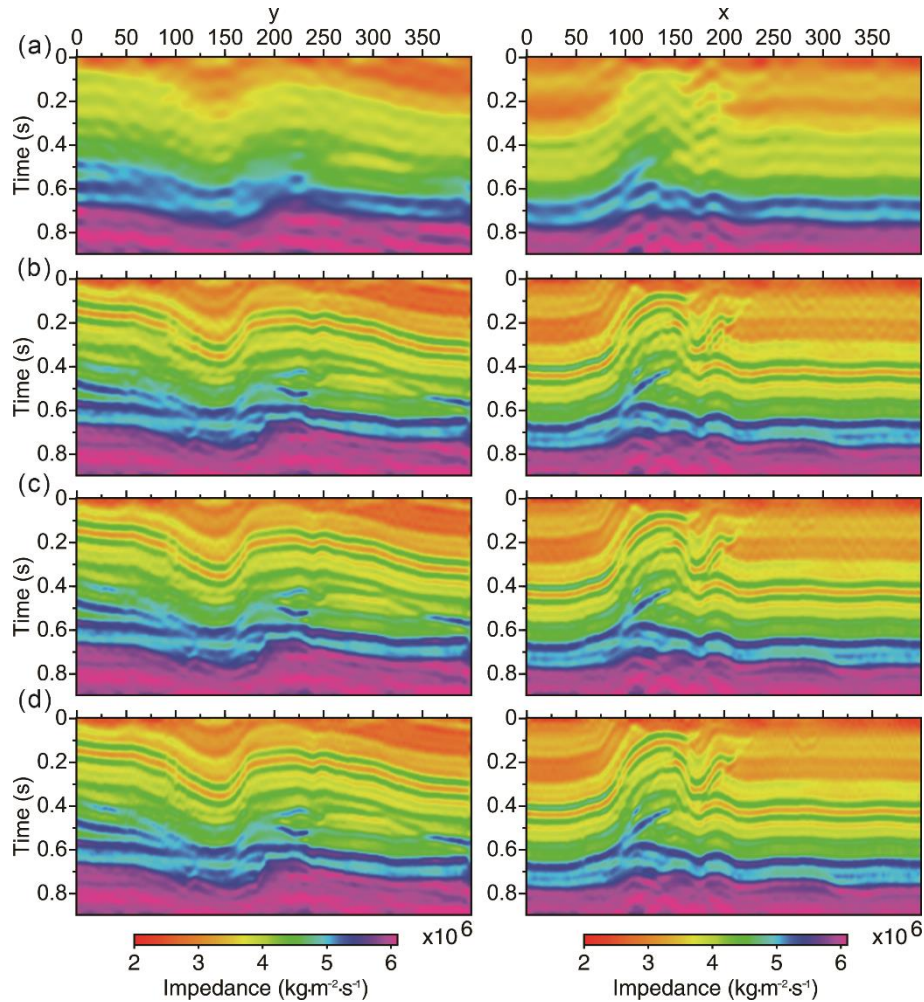
Fig. 6. The inverted impedance profiles when (L, M, N) is equal to (20, 20, 10), (40, 40, 20), (60, 60, 30), and (80, 80, 40) in (a)-(d), respectively. The left and right panels of each subfigures are impedance profiles at $x=100$ and $y=100$, respectively.

We investigate the influences of the values of (L, M, N) and the subgroups on the inverted results in two tests. We chose both the initial values of (L, M, N) and their increments as (10, 10, 5) in the first test and (40, 40, 20) in the second test, and stop the inversion when the values of (L, M, N) reach (80, 80, 40). In each (L, M, N), about 4 subgroups in the first test and 25 subgroups in the second test are used for the inversion of the Fourier coefficients. The other parameters are the same as in Fig. 6. The finally reconstructed impedance model profiles in the two tests (not shown) are almost identical to those in Fig. 6d, but their computation time is about 22 minutes and 52 minutes, respectively. When fewer subsets of data are used in the second test, the time required is reduced but the inverted model is discontinuous. Therefore, considering the inversion results, computational efficiency and convenience of selecting subgroups, we prefer to select about one-tenth of $\left(N_x/2+1, N_y/2+1, N_z/2+1\right)$ as the initial values for (L, M, N), and adjust the subgroups according to the values of (L, M, N) in the inversion.

To test the robustness of the Fourier coefficient-based method when applied to noisy seismic data, we added Gaussian noise to the seismic cube in Fig. 2b. Fig. 9 is the noisy data cube with a signal-to-noise ratio (S/N) of 5. Using the same parameters as for impedance inversion from noise-free data, the inverted impedance profiles using the trace-by-trace method and the Fourier coefficient-based method are shown in Fig. 10a and Fig.10b, respectively. It is obvious that the latter method gives more continuous and stable results of the inverted impedance.
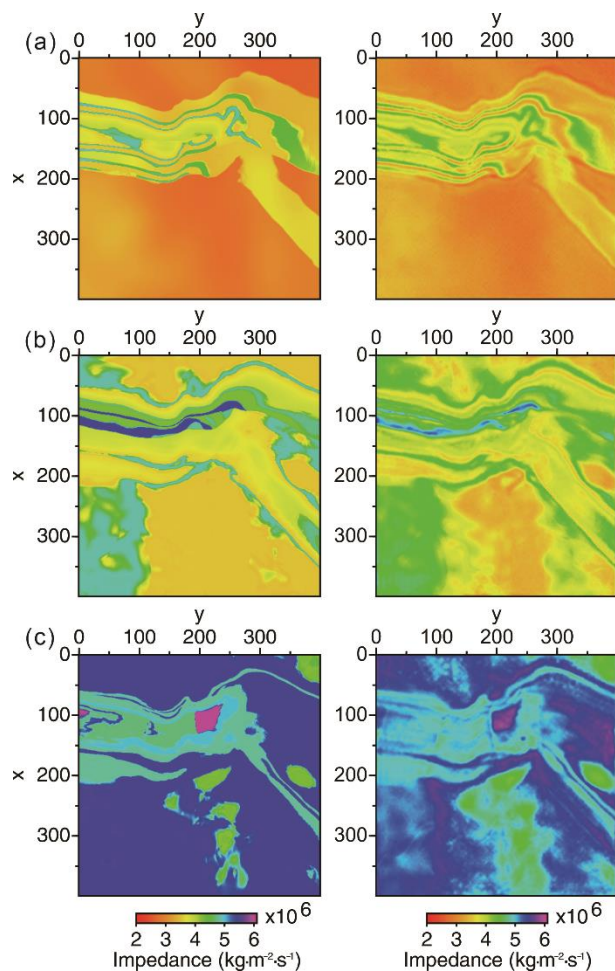
This article has been accepted for publication in IEEE Transactions on Geoscience and Remote Sensing. This is the author's version which has not been fully edited and content may change prior to final publication. Citation information: DOI 10.1109/TGRS.2023.3268410

TGRS-2022-04884

Fig. 7. The slices of the impedance model. (a), (b), and (c).are slices at 0.24 s, 0.45 s and 0.66 s, respectively. Subfigures in the left and right panels are the true and inverted impedance model slices, respectively.

In earlier tests, about 15% of all traces (160,000) were missing. Here we show another case where about 70% of the traces are missing and 50673 non-null traces are involved in the inversion. The results are shown in Fig. 11. It can be seen that the model profiles inverted with the Fourier coefficient-based method, shown in Fig. 11a, are more stable and continuous than those inverted with the trace-by-trace method, shown in Fig. 11b. Comparing to other spatial continuity enhancing methods [17], our method is independent on the a priori geologic information, works well for 3D seismic cube with more missing traces, and is affordable for seismic cube with realistic size.

D. Field seismic data example

Fig. 12a is 3D seismic cube from the carbonate area, which is a post-stack data after migration, and the target zone is approximately between 6 and 7 km. There are 302 traces in both x and y directions, with 19026 missing traces. Each trace contains 251 samples with a time interval of 2 ms and a time range of 3.8 to 4.3 s. The size of the impedance model is $N_x = N_y = 302$, and $N_z = 110$. In this field data example, N_x corresponds to the trace number in the x direction, ranging from 0 to 301, N_y corresponds to the trace number in the y direction, varying from 0 to 301, and the vertical index N_z is the impedance sample number, which ranges from 3.662 s to 4.316 s with an interval of 6 ms. Note that impedance values in between 3.662 s and 3.8 s are equal to the impedance value at 3.8 s in each trace, to remove the direct wave. Fig. 12b is the estimated wavelet from the seismic cube by the generalized wavelet method [18]. Fig. 12c is a spectral profile at x=130, and it can be seen that the frequency range of the field data is about 8–25 Hz. This is because the target zone is located deep below the surface. Influences such as absorption result to the amplitudes of high frequencies of the seismic cube with relatively low values. In the target area, there are two well-logs at (x, y) = (87, 22) and (258, 147) with time range of 4.0–4.2s and 3.92–4.12s, respectively, and three horizons at about 3.8 s, 3.9 s and 4.2 s.

It can be seen that in the target area, the seismic cube is lack of low and high frequency components, and the well and horizontal information are very limited. Besides, since the target layer is deep under the surface, reliable geological information with high resolution is not available. Therefore, to make the inversion results reliable, we will not blindly pursued high resolution with such kind of field data.

In the inversion, to reduce the influence of the lack of low frequencies, we built the initial impedance model using two well-logs and three horizons. Fig. 13a shows the profiles of the initial impedance model at x=258 and y=147, which include the low-wavenumber components, and then we apply the Fourier coefficient-based method for impedance inversion.

The initial values of (L, M, N) and their increments are (15, 15, 8). The final number of terms in the truncated Fourier series is (L, M, N) = (60, 60, 32). For the four (L, M, N), the time required for a coefficient to model calculation using the inverse direct Fourier series method is 1.3, 11.0, 47.5, and 95.3 minutes, respectively, while the corresponding time required using the FFT-based method is only 0.9 seconds.
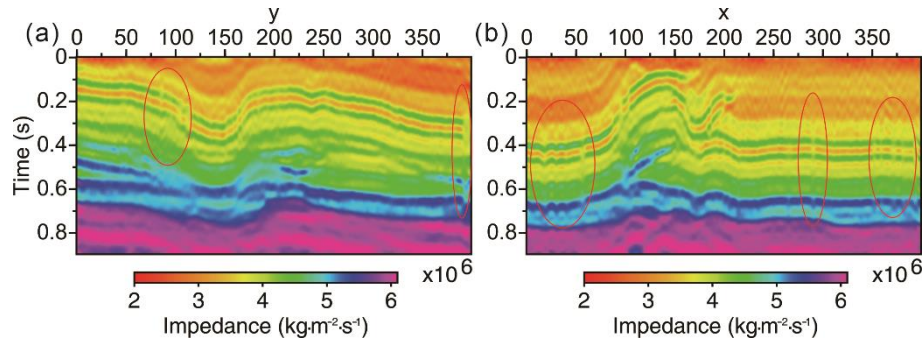
Fig. 8. The inverted impedance profiles at $x=100$ (a) and $y=100$ (b). The subgroup of seismic data used in this inversion is selected every 10 traces in x and y directions from the whole cube.
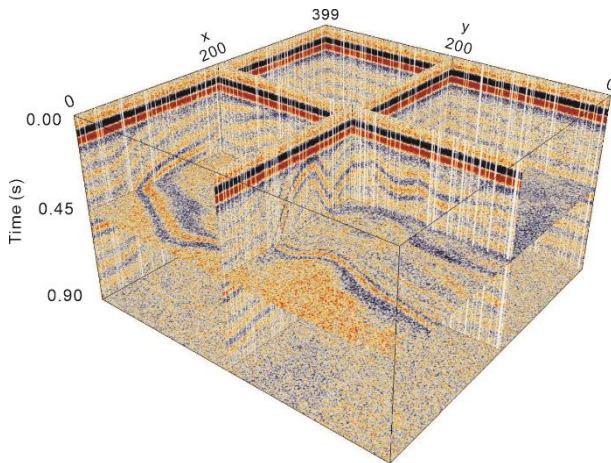

The seismic cube is divided into 16 subgroups, and each of them consists of traces selected every 4 traces along the x- and y- directions. In the parallel implementation, 40 threads are used and the computation time cost is 7.0 minutes. The time saving is much greater than the direct Fourier series method, which is 2600 minutes (43.3 hours). Fig. 13b and 13c show two reconstructed impedance profiles for $(L, M, N) = (30, 30, 16)$ and $(60, 60, 32)$. The latter shows that the inverted impedance profiles have high resolution and good spatial continuity.

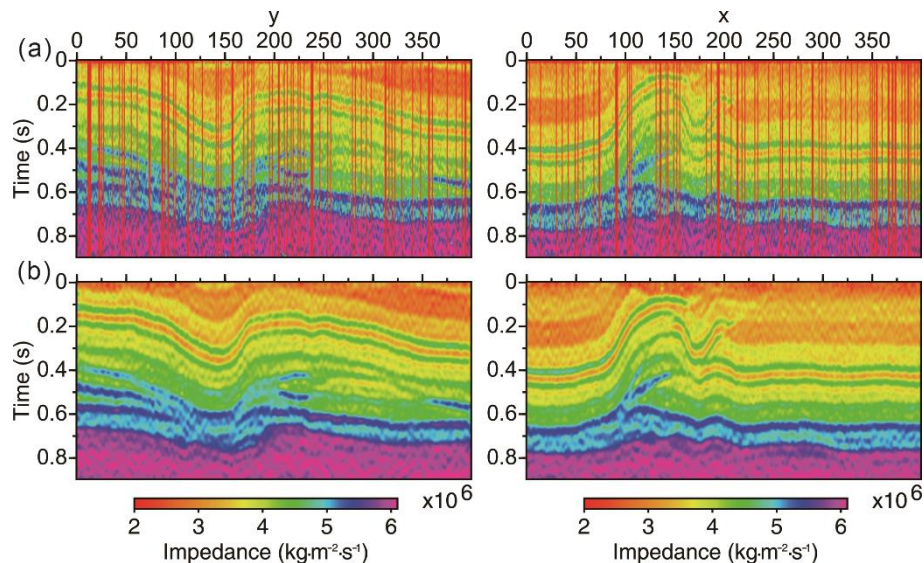Fig. 9. The noise contaminated seismic data with S/N=5.

Fig. 10. The inverted impedance profiles from the noise contaminated data in Fig. 9 by the trace by trace method (a) and Fourier coefficients based method (b). The left and right panels of each subfigures are impedance profiles at $x=100$ and $y=100$, respectively.
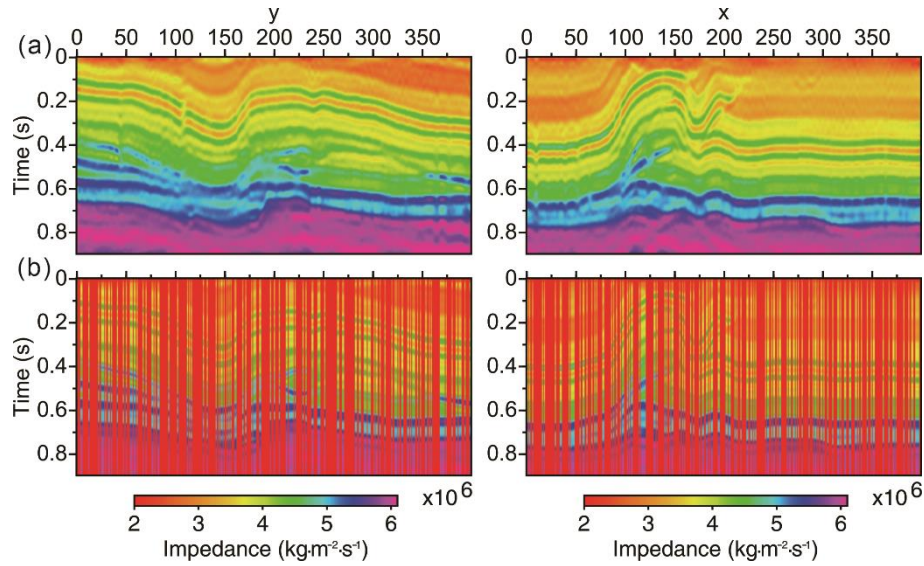
Fig. 11. The inverted impedance profiles by Fourier coefficients based method (a) and the trace by trace method (b). In this case, about 70% of all the traces are missing. The left and right panels of each subfigures are impedance profiles at $x=100$ and $y=100$, respectively.
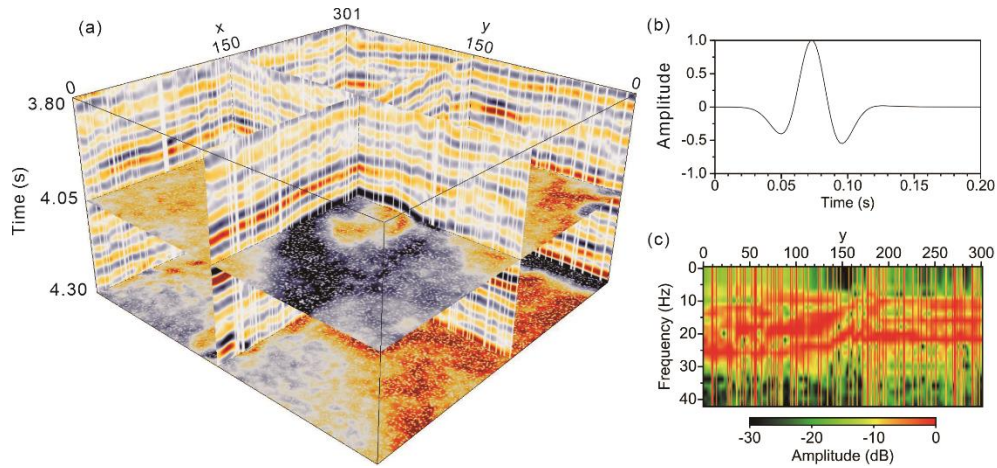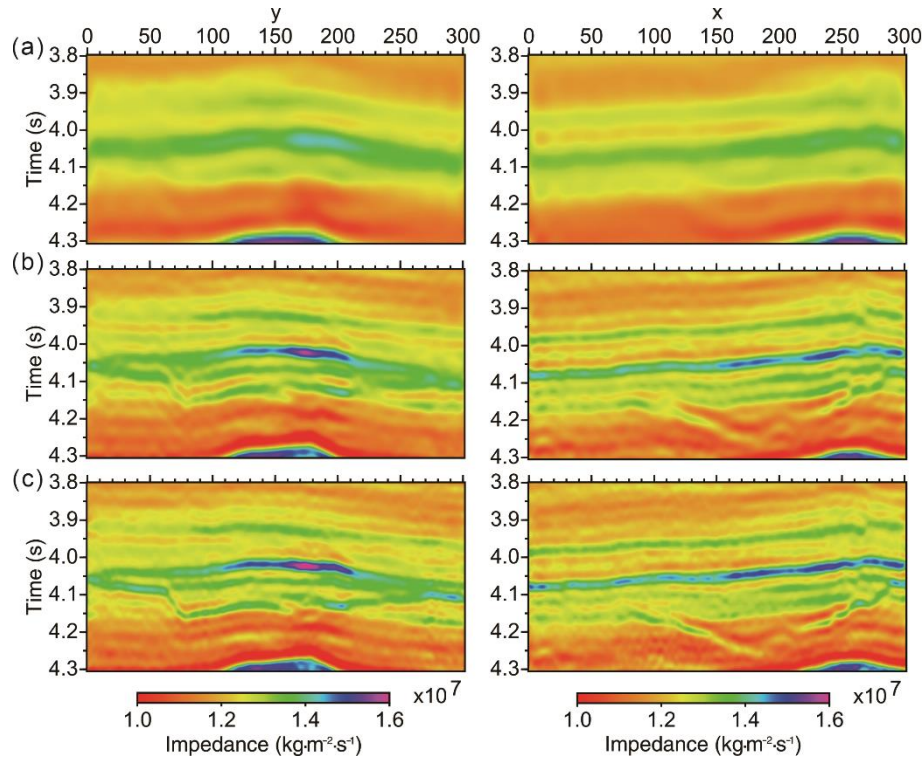

Fig. 12. (a) A field 3D migrated seismic cube. (b) Estimated seismic wavelet from the seismic cube with reference frequency of 16.5 Hz and fractional number $u = 2.16$. (c) Spectral profile at $x=130$ with the frequency range of about 8–25 Hz.

Fig. 13. (a) The initial impedance profiles at x=258 and y=147. (b) The reconstructed impedance profiles when (L, M, N) = (30, 30, 16). (c) The reconstructed impedance profiles when (L, M, N) = (60, 60, 32).

In Fig. 14, we compare the observed traces with the synthetic traces generated by the initial and inverted impedance models, respectively. We see that the synthetic traces generated by the inverted impedance model agree well with the observed traces.
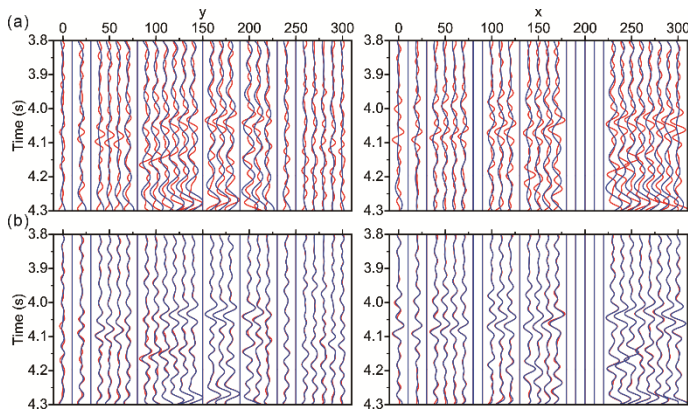
Fig. 14. Comparisons between the observed (red curves) and synthetic (blue curves) traces. The synthetic traces are generated by the initial impedance model (a) and the inverted impedance model when (L, M, N) = (60, 60, 32) (b). The left panels are at x=258 and the right panels are at y=147.

VII. CONCLUSION

In seismic inversion, we can parameterize the 3D model of the subsurface using a truncated Fourier series. In this study, we proposed to determine the coefficients of the truncated Fourier series using forward FFT and reconstruct a 3D model from the inverted Fourier series using inverse FFT. Using the pair of forward and inverse FFT ensures the accuracy of both model fitting and reconstruction. Due to the fast implementation of the FFT pair, the efficiency is greatly improved by this model parameterization scheme. This makes the seismic inversion of the subsurface model affordable for 3D seismic data with a realistic size.

In seismic inversion with model parameterization using truncated Fourier series, we can invert fewer parameters because the number of Fourier coefficients to be inverted is much smaller than that of the model. We can also design inversion strategies to invert the Fourier coefficients from small-valued numbers to large-valued numbers for (L, M, N). In this way we can not only reconstruct the models step by step from low wavenumber components to high wavenumber components, but also save computation time and improve efficiency.

When applied to 3D seismic impedance inversion, this model parameterization scheme can provide continuous and stable impedance results from seismic cubes with missing traces and noise. This is because the impedance model is reconstructed from the Fourier coefficients and each of them is inverted by all the seismic traces used, i.e. the Fourier coefficients are updated in a way that includes multiple traces. Furthermore, in this way the seismic cube is divided into subsets, only a part of which is used for the inversion of the coefficients, resulting in a considerable saving of computational time.

APPENDIX

FORMULAE OF FOURIER COEFFICIENTS OF A 3D PERIODIC FUNCTION

To deduce the Fourier coefficients formulas, one may start from a periodic function $u(x, y, z)$ with the ranges of $\{\, 0 \leq x \leq X, 0 \leq y \leq Y, 0 \leq z \leq Z \,\}$, where $\{\, X, Y, Z \,\}$ are the length of the period function in x, y, and z direction. The formula for the Fourier series expansion of $u(x, y, z)$ has a similar form as (1) [19]. After setting $L = M = N = \infty$ in (1), $\Delta k_x = 2\pi/X$, $\Delta k_y = 2\pi/Y$, $\Delta k_z = 2\pi/Z$ in (3), and changing $\{\, p \to x, q \to y, r \to z \,\}$ in (2), we will have the Fourier series expansion formula for $u(x, y, z)$.

To calculate the Fourier series coefficients, such as a_{lmn}, we multiply $\cos(l\Delta k_x x)\cos(m\Delta k_y y)\cos(n\Delta k_z z)$ to both sides of the Fourier series expansion equation for $u(x, y, z)$, and then integrate both sides over the ranges of $\{\, 0 \leq x \leq X, 0 \leq y \leq Y, 0 \leq z \leq Z \,\}$. Based on the orthogonality of the sine and cosine bases, the formula for a_{lmn} will be derived. The rest Fourier coefficients are derived in the same way. Subsequently, we discretize these formulas for the Fourier coefficients to get their discrete forms.

Note that in the discrete forms, $\{\, \Delta k_x, \Delta k_y, \Delta k_z \,\}$ are following (3). When $\{\, l > 0, m > 0, n > 0 \,\}$, the nonzero valued Fourier coefficients are

$$a_{lmn} = 8\alpha \sum_{(p,q,r)=(0,0,0)}^{(N_x-1,N_y-1,N_z-1)} u(p,q,r)\cos(l\Delta k_x p)\cos(m\Delta k_y q)\cos(n\Delta k_z r),$$

$$b_{lmn} = 8\alpha \sum_{(p,q,r)=(0,0,0)}^{(N_x-1,N_y-1,N_z-1)} u(p,q,r)\sin(l\Delta k_x p)\cos(m\Delta k_y q)\cos(n\Delta k_z r),$$

$$c_{lmn} = 8\alpha \sum_{(p,q,r)=(0,0,0)}^{(N_x-1,N_y-1,N_z-1)} u(p,q,r)\cos(l\Delta k_x p)\sin(m\Delta k_y q)\cos(n\Delta k_z r),$$

$$d_{lmn} = 8\alpha \sum_{(p,q,r)=(0,0,0)}^{(N_x-1,N_y-1,N_z-1)} u(p,q,r)\sin(l\Delta k_x p)\sin(m\Delta k_y q)\cos(n\Delta k_z r),$$

$$e_{lmn} = 8\alpha \sum_{(p,q,r)=(0,0,0)}^{(N_x-1,N_y-1,N_z-1)} u(p,q,r)\cos(l\Delta k_x p)\cos(m\Delta k_y q)\sin(n\Delta k_z r),$$

$$f_{lmn} = 8\alpha \sum_{(p,q,r)=(0,0,0)}^{(N_x-1,N_y-1,N_z-1)} u(p,q,r)\sin(l\Delta k_x p)\cos(m\Delta k_y q)\sin(n\Delta k_z r),$$

$$g_{lmn} = 8\alpha \sum_{(p,q,r)=(0,0,0)}^{(N_x-1,N_y-1,N_z-1)} u(p,q,r)\cos(l\Delta k_x p)\sin(m\Delta k_y q)\sin(n\Delta k_z r),$$

$$h_{lmn} = 8\alpha \sum_{(p,q,r)=(0,0,0)}^{(N_x-1,N_y-1,N_z-1)} u(p,q,r)\sin(l\Delta k_x p)\sin(m\Delta k_y q)\sin(n\Delta k_z r).$$

(A-1)

where $\alpha = 1/(N_x N_y N_z)$.

When $l = 0, m > 0, n > 0$, the nonzero valued Fourier coefficients are

$$a_{0mn} = 4\alpha \sum_{(p,q,r)=(0,0,0)}^{(N_x-1,N_y-1,N_z-1)} u(p,q,r)\cos(m\Delta k_y q)\cos(n\Delta k_z r),$$

$$c_{0mn} = 4\alpha \sum_{(p,q,r)=(0,0,0)}^{(N_x-1,N_y-1,N_z-1)} u(p,q,r)\sin(m\Delta k_y q)\cos(n\Delta k_z r),$$

$$e_{0mn} = 4\alpha \sum_{(p,q,r)=(0,0,0)}^{(N_x-1,N_y-1,N_z-1)} u(p,q,r)\cos(m\Delta k_y q)\sin(n\Delta k_z r),$$

$$g_{0mn} = 4\alpha \sum_{(p,q,r)=(0,0,0)}^{(N_x-1,N_y-1,N_z-1)} u(p,q,r)\sin(m\Delta k_y q)\sin(n\Delta k_z r).$$

(A-2)

When $\{\, m = 0, l > 0, n > 0 \,\}$, the nonzero valued Fourier coefficients are

$$a_{l0n} = 4\alpha \sum_{(p,q,r)=(0,0,0)}^{(N_x-1,N_y-1,N_z-1)} u(p,q,r)\cos(l\Delta k_x p)\cos(n\Delta k_z r),$$

$$b_{l0n} = 4\alpha \sum_{(p,q,r)=(0,0,0)}^{(N_x-1,N_y-1,N_z-1)} u(p,q,r)\sin(l\Delta k_x p)\cos(n\Delta k_z r),$$

$$e_{l0n} = 4\alpha \sum_{(p,q,r)=(0,0,0)}^{(N_x-1,N_y-1,N_z-1)} u(p,q,r)\cos(l\Delta k_x p)\sin(n\Delta k_z r),$$

$$f_{l0n} = 4\alpha \sum_{(p,q,r)=(0,0,0)}^{(N_x-1,N_y-1,N_z-1)} u(p,q,r)\sin(l\Delta k_x p)\sin(n\Delta k_z r).$$

(A-3)

When $\{\, n = 0, l > 0, m > 0 \,\}$, the nonzero valued Fourier coefficients are

$$a_{lm0} = 4\alpha \sum_{(p,q,r)=(0,0,0)}^{(N_x-1,N_y-1,N_z-1)} u(p,q,r)\cos(l\Delta k_x p)\cos(m\Delta k_y q),$$

$$b_{lm0} = 4\alpha \sum_{(p,q,r)=(0,0,0)}^{(N_x-1,N_y-1,N_z-1)} u(p,q,r)\sin(l\Delta k_x p)\cos(m\Delta k_y q),$$

$$c_{lm0} = 4\alpha \sum_{(p,q,r)=(0,0,0)}^{(N_x-1,N_y-1,N_z-1)} u(p,q,r)\cos(l\Delta k_x p)\sin(m\Delta k_y q),$$

$$d_{lm0} = 4\alpha \sum_{(p,q,r)=(0,0,0)}^{(N_x-1,N_y-1,N_z-1)} u(p,q,r)\sin(l\Delta k_x p)\sin(m\Delta k_y q).$$

(A-4)

When $\{\, l = m = 0, n > 0 \,\}$ or $\{\, l = n = 0, m > 0 \,\}$ or $\{\, m = n = 0, l > 0 \,\}$, the nonzero valued Fourier coefficients are

$$a_{00n} = 2\alpha \sum_{(p,q,r)=(0,0,0)}^{(N_x-1,N_y-1,N_z-1)} u(p,q,r)\cos(n\Delta k_z r),$$

$$a_{0m0} = 2\alpha \sum_{(p,q,r)=(0,0,0)}^{(N_x-1,N_y-1,N_z-1)} u(p,q,r)\cos(m\Delta k_y q),$$

$$a_{l00} = 2\alpha \sum_{(p,q,r)=(0,0,0)}^{(N_x-1,N_y-1,N_z-1)} u(p,q,r)\cos(l\Delta k_x p),$$

$$b_{l00} = 2\alpha \sum_{(p,q,r)=(0,0,0)}^{(N_x-1,N_y-1,N_z-1)} u(p,q,r)\sin(l\Delta k_x p),$$

$$c_{0m0} = 2\alpha \sum_{(p,q,r)=(0,0,0)}^{(N_x-1,N_y-1,N_z-1)} u(p,q,r)\sin(m\Delta k_y q),$$

$$e_{00n} = 2\alpha \sum_{(p,q,r)=(0,0,0)}^{(N_x-1,N_y-1,N_z-1)} u(p,q,r)\sin(n\Delta k_z r).$$

$$(A-5)$$

When $\{ l = m = n = 0 \}$, we have

$$a_{000} = \alpha \sum_{(p,q,r)=(0,0,0)}^{(N_x-1, N_y-1, N_z-1)} u(p,q,r). \qquad (A-6)$$

REFERENCES

[1] Y. Wang, and R. G. Pratt, "Sensitivities of seismic traveltimes and amplitudes in reflection tomography", *Geophys. J. Int.*, vol. 131, pp. 618–642, Dec. 1997, doi: 10.1111/j.1365-246X.1997.tb06603.x.

[2] Y. Wang, and A. G. Houseman, "Inversion of reflection seismic amplitude data for interface geometry," *Geophys. J. Int.*, vol. 117, no. 1, pp. 92–110, Apr. 1994, doi: 10.1111/j.1365-246X.1994.tb03305.x

[3] Y. Wang, and A. G. Houseman, "Tomographic inversion of reflection seismic amplitude data for velocity variation," *Geophys. J. Int.*, vol. 123, no. 2, pp. 355–372, Nov. 1995, doi: 10.1111/j.1365-246X.1995.tb06859.x.

[4] Y. Wang, "Simultaneous inversion for model geometry and elastic parameters," *Geophys.*, vol. **64**, no. 1, pp. 182–190, Feb. 1999, doi: 10.1190/1.1444514.

[5] Y. Wang, and R. G. Pratt, "Seismic amplitude inversion for interface geometry of multi-layered structures," *Pure Appl. Geophys.*, vol. 157, pp. 1601–1620, Oct. 2000, doi: 10.1007/PL00001052.

[6] Y. Wang, *Seismic Inversion, Theory and Applications*. Oxford, UK: Wiley Blackwell, 2016, pp. 187-201.

[7] J. Liu, and Y. Wang, "Seismic simultaneous inversion using a multidamped subspace method," *Geophysics*, vol. 85, no. 1, pp. R1–R10, Jan. 2020, doi: 10.1190/geo2018-0470.1.

[8] I. Loris, G. Nolet, I. Daubechies, and F. A. Dahlen, "Tomographic inversion using L1-norm regularization of wavelet coefficients," *Geophys. J. Int.*, vol. 170, no. 1, pp. 359–370, July 2007, doi: 10.1111/j.1365-246X.2007.03409.x.

[9] M. Aleardi, and A. Salusti, "Elastic prestack seismic inversion through discrete cosine transform reparameterization and convolutional neural networks," *Geophysics*, vol. 86, no. 1, pp. R129–R146, Jan. 2021, doi: 10.1190/geo2020-0313.1.

[10] D. Lee, J. Lee, C. Shin, S. Shin, and W. Chung, "Elastic full-waveform inversion using both the multiparametric approximate hessian and the discrete cosine transform," *IEEE Trans. Geosci. Remote Sens.*, vol. 60, pp. 1–10, Aug. 2022, doi: 10.1109/TGRS.2021. 3101193.

[11] R. Nunes, L. Azevedo, and A. Soares, "Fast geostatistical seismic inversion coupling machine learning and Fourier decomposition," *Computat. Geosci.*, vol. 23, pp. 1161–1172, Aug. 2019, doi: 10.1007/s10596-019-09877-w.

[12] A. Jeffrey, *Advanced Engineering Mathematics*. Harcourt/Academic Press, 2002.

[13] M. Frigo, and S. G. Johnson, "The design and implementation of FFTW3," *Proc. IEEE*, vol. 93, no. 2, pp. 216–231, Feb. 2005, doi: 10.1109/JPROC.2004.840301.

[14] A. Tarantola, "Inversion of seismic reflection data in the acoustic approximation," *Geophysics*, vol. 49, no. 1, pp. 1259–1266, Aug. 1984, doi: 10.1190/1.1441754.

[15] A. Tarantola, "A strategy for nonlinear elastic inversion of seismic reflection data," *Geophysics*, vol. **51**, no. 10, pp. 1893−1903, Nov. 1986, doi: 10.1190/1.1442046.

[16] D. Vigh, E.W. Starr, and J. Kapoor, "Developing earth models with full waveform inversion," *The Lead. Edge*, vol. 28, no. 4, pp. 432–435, Apr. 2009, doi: 10.1190/1.3112760.

[17] R. G. Clapp, B. Biondi, and J. F. Claerbout, "Incorporating geologic information into reflection tomography," *Geophysics*, vol. 69, no. 2, pp. 533–546, Jan. 2004, doi: 10.1190/1.1707073.

[18] Y. Wang, "Generalized seismic wavelets," *Geophys. J. Int.*, vol. 203, no. 2, pp. 1172–1178, Nov. 2015, doi:10.1093/gji/ggv346.

[19] Y. Wang, *Seismic Amplitude Inversion in Reflection Tomography*. Pergamon/Elsevier, Feb. 2003.